

LETTER TO THE EDITOR

Hard x-ray and hot electron production from intense laser irradiation of wavelength-scale particles

T D Donnelly¹, M Rust¹, I Weiner¹, M Allen², R A Smith³, C A Steinke⁴,
S Wilks⁵, J Zweiback⁵, T E Cowan⁵ and T Ditmire^{5,6}

¹ Department of Physics, Harvey Mudd College, Claremont, CA, USA

² Department of Nuclear Engineering, University of California, Berkeley, CA, USA

³ Blackett Laboratory, Imperial College, London, UK

⁴ Lyman Laboratory, Harvard University, Cambridge, MA, USA

⁵ Laser Program, Lawrence Livermore National Laboratory, Livermore, CA, USA

Received 20 February 2001, in final form 2 April 2001

Abstract

We have examined the production of hard x-rays from the irradiation of $\sim 1 \mu\text{m}$ diameter water droplets with a 35 fs laser at an intensity of up to $7 \times 10^{17} \text{ W cm}^{-2}$. We observe substantial x-ray production in the photon energy range above 100 keV and find that the implied hot electron temperatures from these micron-scale targets are significantly higher than electron temperatures observed from irradiation of solid planar plastic targets under nearly identical irradiation conditions. The observed enhancement of the hot electron temperature from droplets is consistent with hot electron spectra calculated from particle-in-cell simulations.

Over the last few years, experimental studies have shown that sub-picosecond to femtosecond chirped pulse amplification lasers focused to intensities of 10^{17} – $10^{20} \text{ W cm}^{-2}$ on solid targets can accelerate substantial numbers of electrons to high energy, and that these fast electrons can produce large fluxes of hard x-rays via bremsstrahlung emission in the target [1]. A number of such experiments have observed photons emitted in the $> 1 \text{ MeV}$ energy range indicating that such focused laser intensity can accelerate electrons to relativistic temperatures of several hundred keV to well over a MeV [2–5]. Furthermore, there is now a growing interest in these energetic interactions as a source of hard x-rays for applications which include laser-driven radiography and perhaps laser-driven photo-nuclear processes.

The mechanisms leading to the acceleration of fast electrons responsible for the hard x-rays in laser–solid interactions have been the topic of many experimental and theoretic studies over the past two decades. At intensities approaching $10^{18} \text{ W cm}^{-2}$ the ponderomotive potential of light with wavelength around $1 \mu\text{m}$ nears 100 keV and direct acceleration of electrons can occur through electron interactions with the laser field at a plasma surface (Brunel heating [6]) or through $\mathbf{J} \times \mathbf{B}$ heating [7, 8]. In addition, when a long scale-length (many

⁶ Current address: Department of Physics, University of Texas, Austin, TX 78712, USA.

wavelength) preformed plasma exists in front of the target, collective electron oscillations driven by resonance absorption or stimulated Raman scattering can also play an important role in accelerating the electrons [9]. Generally, both theoretical and experimental evidence indicates a linear or sub-linear scaling of fast electron temperature with laser ponderomotive potential [10, 11] with calculated hot electron distributions for p-polarized pulses incident on solids exhibiting temperature four to five times the laser ponderomotive potential [10]. Other studies have found slightly different scaling laws though the magnitude and mechanisms for the electron heating are consistent [11, 12]. However, virtually all of these experimental and theoretical studies considered laser pulses incident on planar plasma surfaces.

Linear absorption and scattering of light by particles whose size is comparable to the wavelength of light (around $1\ \mu\text{m}$) can be increased over that of bulk media from enhancements in the light field surrounding the sphere; so-called Mie resonances. Thus we might expect that the dynamics of laser-driven electron motion will be quite different around such a wavelength-scale sphere, and that vacuum heating of hot electrons will take on a different character. In this letter, we report on experiments and simulations of such high-intensity irradiation of micron-sized particles with femtosecond pulses. We observe strong x-ray production in the 0.1–1 MeV photon energy range when a spray of micron-scale water droplets is irradiated at an intensity approaching $10^{18}\ \text{W cm}^{-2}$. Measured hard x-ray spectra from the droplet target indicate that hot electron temperatures are nearly twice as high as hot electron temperatures produced from solid, planar targets under very similar irradiation conditions. The observed enhancement of hot electron temperature from the droplets over planar solids is also consistent with two-dimensional particle-in-cell simulations of the interaction.

The experiment was performed with a Ti:sapphire chirped pulse amplification laser delivering 35 fs pulses at 820 nm. For the experiments described here, 0.12 J of laser energy was focused in vacuum with an $f/15$ lens to a focal spot of roughly $20\ \mu\text{m}$ diameter ($1/e^2$). Far-field measurements indicate a peak intensity of $7 \times 10^{17}\ \text{W cm}^{-2}$. The pre-pulse intensity contrast was $\sim 10^{-6}$ on the 1 ns timescale before the main pulse and was $\sim 10^{-4}$ on the 10 ps timescale. We estimate that plasma pre-expansion from pre-pulse light was well under $1\ \mu\text{m}$. These pulses were focused onto either a plane, plastic target in p-polarization at an incidence angle of 10° or into a spray of water droplets. Plastic was chosen as the target material because it exhibits a similar density and has a similar Z value to water, the target material in our droplet spray.

The water droplet target was produced by an apparatus capable of creating a high-density, polydisperse spray containing micron-scale liquid water droplets in vacuum (similar to the apparatus described in [13]). The droplet source consisted of a gas line backed with high-pressure argon (at 67 bar), an inert propellant gas, over a liquid reservoir. The line terminated in a solenoid-driven pulsed valve with a $750\ \mu\text{m}$ orifice. The valve was pulsed for $500\ \mu\text{s}$, causing propellant gas carrying liquid droplets to stream through the orifice.

The composition of the spray produced by the device was characterized in vacuum by measuring the angular scattering and attenuation of a continuous-wave 543 nm helium–neon laser polarized perpendicular to the scattering plane. The droplet sizes were measured by fitting theoretical Mie scattering curves of the 543 nm light to the data [14]. As the radius of the sphere increases, the ratio of the intensity of light scattered in the forward direction increases relative to that scattered at larger angles, making the angular distribution of scatter a sensitive test of particle size. We measured angular scattering from the droplet spray by mounting a photodiode on an arm that was free to rotate on a rotation stage directly beneath the pulsed valve orifice. Several data points were taken at each angle from 3° to 20° in 1° increments. Relative Mie scattering data were obtained by integrating the observed signal over the entire $500\ \mu\text{s}$ open time. Angular scatter data for the droplet spray used in our experiment are shown in figure 1.

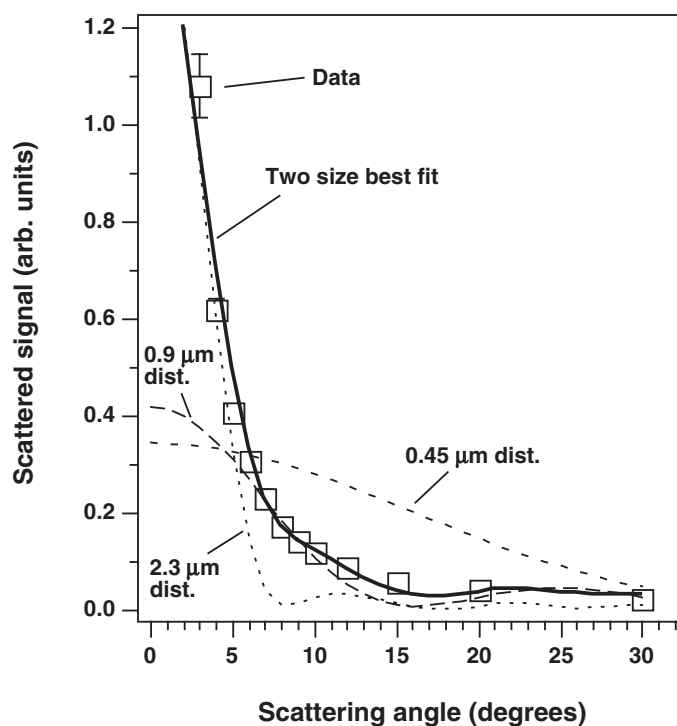


Figure 1. Measured and calculated intensity of scatter from the droplet spray versus angle.

To ascertain the droplet size, we calculate expected scattering angular distributions using a code calculating the differential Mie scattering cross section. We find that we can fit these scattering data if a two size distribution is assumed. A fit with a single size distribution centred at $r = 0.9 \mu\text{m}$ is plotted in the figure. This calculation adequately fits the data at mid-angles (5° – 15°) though it contains oscillations at large angles not seen in the data and does not reproduce the large scattering at small angles. To adequately fit the observed data, we assume a droplet size distribution with a Gaussian profile centred at $r = 0.9 \mu\text{m}$ with a 20% spread (at the $1/e$ point) with a small additional contribution of droplets with $r = 2.3 \mu\text{m}$. The large droplets contribute predominately to the small angle scatter signal. The data are reasonably well reproduced by calculation when we assume that 5% of the droplets have an $r = 2.3 \mu\text{m}$. For comparison, we also show curves for purely $r = 2.3 \mu\text{m}$ droplets as well as small $r = 0.45 \mu\text{m}$.

The droplet density was determined from light attenuation measurements. With knowledge of the droplet size, and the propagation length of the probe laser through the droplet plume (determined by imaging the scattering onto a CCD), one can use Mie theory to calculate the average density of particles in the plume. Our measurements indicate that the droplet spray was roughly 2 mm wide and exhibited a density of 6×10^7 droplets/cm³ (or 7×10^{18} molecules/cm³). This implies that there are a few tens (10–100) of droplets in the focal volume per laser shot.

Hard x-rays from the target region, either droplet or planar solid, were observed 90° from the laser propagation axis using detectors employing NaI crystals coupled to photo-multiplier tubes. These detectors were housed in a thick lead casing with an aperture pointed at the target region. X-rays were observed through a 5 mm thick glass window and data were taken with

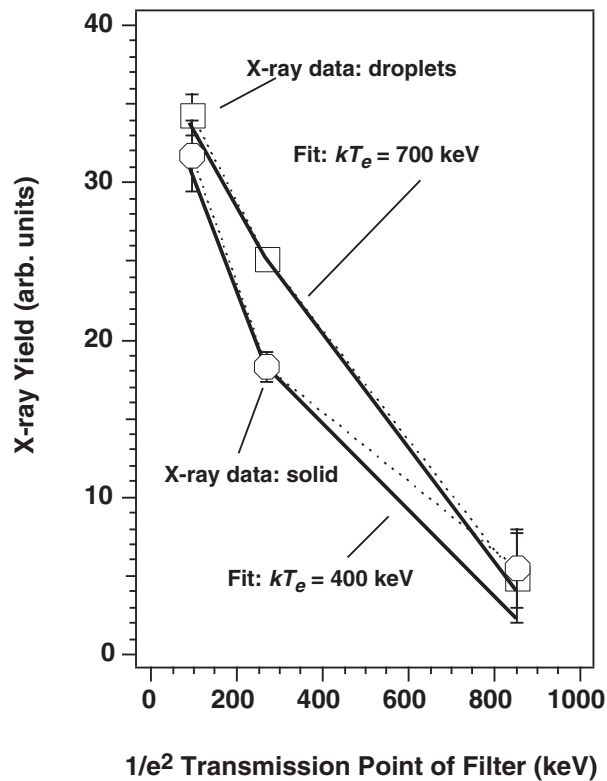


Figure 2. X-ray yield measured in an NaI detector versus filter transmission energy for the droplet target (squares) and the solid plastic target (octagons). The filters used were 0.5 cm Cu (cut-off at 97 keV), 0.35 cm Pb (cut-off at 270 keV), and 4 cm Pb (cut-off at 925 keV). Dashed lines connect the data points; solid, bold lines present best electron temperature fits.

three different filters in front of the detector. We acquired data with an 0.5 cm thick Cu filter and 0.35 and 4 cm thick Pb filters. These filters were chosen to yield spectral information in the 100 keV–1 MeV photon energy range. In addition, data were collected with an unshielded reference detector, filtered by only the 5 mm stainless steel vacuum chamber wall. This detector provided information on x-rays produced with energy above 50 keV and was used to discriminate high- and low-intensity shots.

Abundant hard x-ray emission was observed from both the solid plastic targets and the water droplet target. The x-ray yield measured from both targets is plotted in figure 2. Here the total x-ray energy deposited in the detector per shot is plotted versus the cut-off energy ($1/e^2$) of each filter. Consequently the data points roughly represent the integrated x-ray yield above this photon energy point. From this illustration it is evident that the total x-ray yield observed from the two kinds of targets is comparable over the 0.1–1 MeV energy range. Hard x-rays from the solid target occur due to bremsstrahlung of fast electrons in the bulk material. We further surmise that hard x-ray emission occurs in the droplet target due to bremsstrahlung in the stainless steel droplet jet body from hot electrons produced in the droplets themselves.

While a direct comparison of x-ray yields between these two targets does not yield quantitative information because of the differing mechanisms for producing the bremsstrahlung (plastic as opposed to stainless steel converter for the droplets), it is clear from this figure that the comparable x-ray yields indicate at least roughly comparable hot electron production in

the two cases. Though the production of fast electrons from the micron-scale droplets is not entirely unexpected with the potential for Brunel heating, it is interesting in light of the fact that we observe no measurable hard x-ray production from large van der Waals clusters. We examined yields when a gas of Xe clusters of roughly 30 nm (1–2% of the size of the droplets used in our experiment) was irradiated under identical conditions and measured no x-rays through any of the x-ray filters. This result suggests a clear difference in the nature of the laser-field–fast-electron interaction as the particle size approaches the laser wavelength.

To determine the approximate hot electron temperature from these data, we performed simulations of bremsstrahlung production from various exponential electron distributions using the Monte Carlo code, ITS [15]. We calculate hard x-ray spectra from single temperature electron distributions in plastic and in solid iron (to model the droplet x-ray production) and account for the target geometry and direction of detection (90° to the laser). We assume a single-temperature Maxwellian electron energy distribution and numerically generated a photon spectrum, $f(E_\gamma) dE_\gamma$ where E_γ is the photon energy. These results were then fitted to the data points using a least squares analysis by varying the initial hot electron temperature using the fact that the signal measured in each filtered detector is proportional to $\int E_\gamma T(E_\gamma) f(E_\gamma) dE_\gamma$ where $T(E_\gamma)$ is the transmission of each filter as a function of x-ray wavelength.

The best spectrum for each of the targets is also shown in figure 2. We find that the best-fit hot electron temperature of the solid plastic target is 400 keV with a single standard deviation of ± 100 keV. The droplet target data exhibited a best fit with a 700 keV hot electron temperature and a standard deviation of ± 150 keV. The temperature of the solid target is consistent with previously published hot electron temperature measurements in this intensity range (approaching $10^{18} \text{ W cm}^{-2}$) [2, 16], however, the hot electron temperature inferred from the droplet measurements is nearly twice that inferred from the solid target.

To understand these observed differences, we have also conducted two-dimensional particle-in-cell simulations of a 30 fs pulse irradiating a round solid density plasma and planar solid targets at a peak intensity of $5 \times 10^{17} \text{ W cm}^{-2}$. These simulations were conducted with the code ZOHAR [17] in which solid material was approximated as an overdense, $5 \times 10^{22} \text{ cm}^{-3}$ plasma. In the planar target calculations, the laser field was p-polarized and was incident at an angle of 19° . In these simulations we observe the presence of enhanced regions of electric field near the droplet surface in a roughly dipole pattern (i.e. both at the surface of incidence as well as the back surface). An example of the field distribution calculated around a $1 \mu\text{m}$ spherical (droplet) plasma is shown as a contour plot in figure 3(a) near the peak of the laser pulse envelope. This arises from the oscillating electrons perpendicular to the laser k vector. The hot electron spectra produced from simulations of the droplet and the planar slab are shown in figure 3(b). The calculation predicts a hot electron temperature of 125 keV from the flat target and a temperature of 240 keV from the droplet, nearly a factor of two higher than the planar slab, much like the enhancement observed in the experiments. Though these electron temperatures are somewhat lower than observed in the experiment, they do confirm that the electron temperature resulting from the interaction with a small sphere is significantly higher than in the interaction with a planar slab.

In the simulation, the majority of the hot electron production is due to Brunel-type heating of the oscillating electrons at the surface in both the droplet and the slab target simulations. However, the enhanced electron heating observed in the case of the particle appears to arise from the differing electron trajectories possible around the droplet target geometry. In the case of the slab target, electrons acquire energy from the laser field through acceleration in vacuum toward the slab surface. Thus, most electrons acquire substantial velocity in the direction perpendicular to the slab surface (the direction in which the field adiabaticity is broken). In the droplet simulation, however, the laser field diffracts around the droplet and electrons can

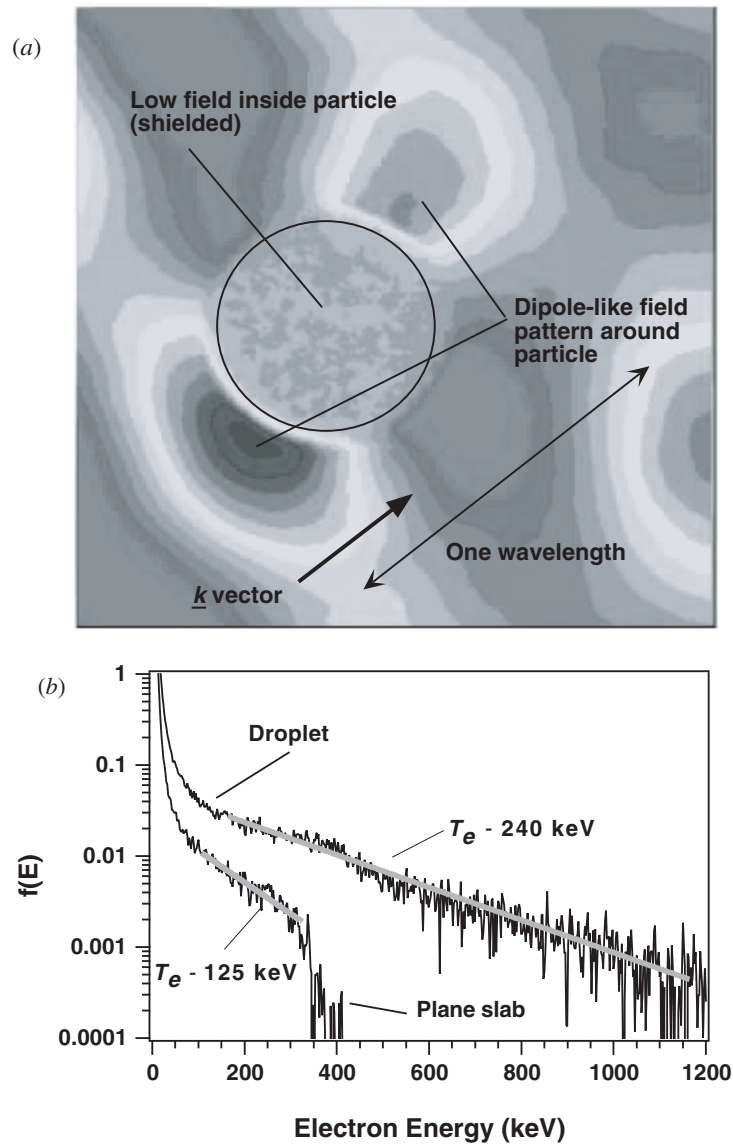


Figure 3. (a) Contour plot of the magnitude of the electric field around a $1 \mu\text{m}$ diameter solid density plasma droplet as calculated by the particle-in-cell simulation ZOHAR. The distribution is shown at the peak of the 30 fs incident laser pulse with a peak intensity of $5 \times 10^{17} \text{ W cm}^{-2}$. (b) Calculated hot electron spectra calculated by the particle-in-cell simulation ZOHAR from the interaction of a 30 fs incident laser pulse with peak intensity of $5 \times 10^{17} \text{ W cm}^{-2}$ with a $1 \mu\text{m}$ diameter solid density plasma droplet and with a planar slab. The light grey lines represent best Maxwellian fits to the calculated spectra. (c) Plots of momentum in the x and y directions of electrons in both simulations. The x direction is the direction perpendicular to the slab surface (the laser k vector is 19° off from this direction in both cases). The spatial extent in x of both the droplet and slab can be seen from the concentration of low-energy electrons.

undergo numerous surface penetrations at various angles through the surface of the plasma sphere. In this case, the particle plasma is large enough to shield the laser field (unlike the case

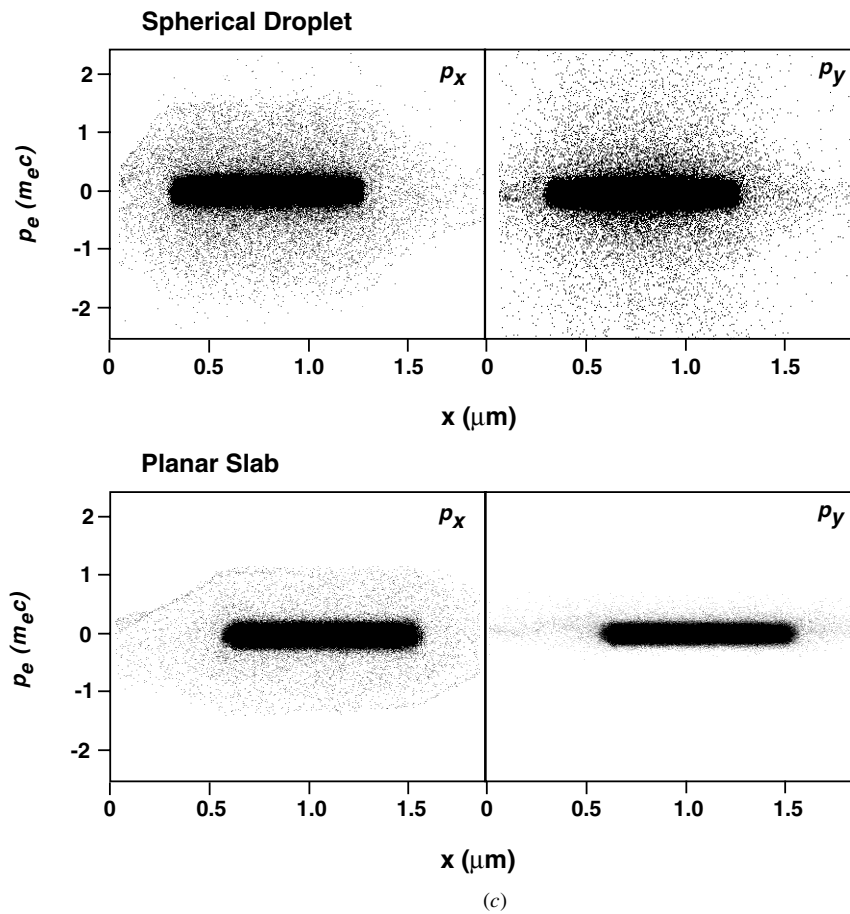


Figure 3. Continued.

of the much smaller nanometre-scale clusters studied) and the electrons can acquire substantial momentum, both parallel and perpendicular to the laser k direction.

This effect is illustrated in figure 3(c) in which the momentum of the electrons in the two directions is plotted as a function of position, x (where the x direction is perpendicular to the planar slab surface). Momentum plots at the end of the laser pulse for both droplet (top) and slab (bottom) are shown. (The large concentration of particles in the centre of the plots are the low-energy, <10 keV electrons.) While the droplet shows fast particles in both directions (with momentum of $>1.0m_e c$) the slab simulation shows that electrons are accelerated to high velocity only in the x direction. Virtually no particles with $p_y > 0.5m_e c$ are observed in the case of the slab.

In conclusion, we have measured hard x-ray yield from femtosecond laser interactions with both solid and micron-scale droplet targets. Strong hard x-ray production is observed from both targets. However, the inferred electron temperature is somewhat higher in the case of irradiation of the droplets. These data are consistent with particle-in-cell simulations. This finding indicates that quite unique hot electron dynamics occur during the irradiation of wavelength-scale particles by an intense laser field and likely warrants further study.

This work was performed under the auspices of the DOE, contract W-7405-Eng-48. This work was partially supported by the donors of the Petroleum Research Fund, administered by the American Chemical Society, and the Research Corporation. We would like to acknowledge the technical assistance of G Hays, G Anderson, V Tsai, R Shuttlesworth, and M Wheeler.

References

- [1] Kmetec J D *et al* 1992 *Phys. Rev. Lett.* **68** 1527
- [2] Gahn C *et al* 1998 *Appl. Phys. Lett.* **73** 3662
- [3] Chichkov B N *et al* 1996 *Appl. Phys. Lett.* **68** 2804–6
- [4] Ikhlef A, Jiang Z, Kieffer J C and Krol A 1998 *J. X-Ray Sci. Technol.* **8** 151
- [5] Schnurer M *et al* 1995 *Phys. Plasmas* **2** 3106
- [6] Brunel F 1987 *Phys. Rev. Lett.* **59** 52
- [7] Kruer W L and Estabrook K 1985 *Phys. Fluids* **28** 430
- [8] Wilks S C, Kruer W L, Tabak M and Langdon A B 1992 *Phys. Rev. Lett.* **69** 1383
- [9] Estabrook K and Kruer W L 1983 *Phys. Fluids* **26** 1892
- [10] Wilks S C 1993 *Phys. Fluids B* **5** 2603–8
- [11] Gibbon P 1994 *Phys. Rev. Lett.* **73** 664
- [12] Bell A R, Davies J R, Guerin S and Ruhl H 1997 *Plasma Phys. Control. Fusion* **39** 653
- [13] Mountford L C, Smith R A and Hutchinson M H R 1998 *Rev. Sci. Instrum.* **69** 3780
- [14] Kerker M 1969 *Scattering of Light and Other Electromagnetic Radiation* (New York: Academic)
- [15] Halbleib J A and Mehlhorn T A 1986 *Nucl. Sci. Eng.* **92** 338
- [16] Malka G and Miquel J L 1996 *Phys. Rev. Lett.* **77** 75
- [17] Langdon A B and Lasinski B F 1976 *Methods in Computational Physics* vol 16 (New York: Academic) p 327